IEEE Photonics Journal
An IEEE Photonics Society Publication

Broadband Extended Dynamic Range Analog Signal Transmission Through Switched Dual Photonic Link Architecture

Volume 3, Number 1, February 2011

Manik Attygalle, Member, IEEE
Kamal Gupta
Tim Priest

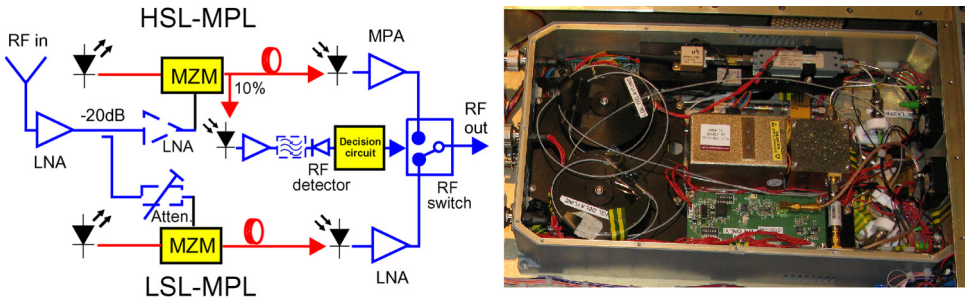

Schematic for the extended dynamic range MPL with dual link architecture and the practical implementation of the transceiver.

DOI: 10.1109/JPHOT.2011.2106200
1943-0655/$26.00 ©2011 IEEE

Broadband Extended Dynamic Range Analog Signal Transmission Through Switched Dual Photonic Link Architecture

Manik Attygalle, *Member, IEEE*, Kamal Gupta, and Tim Priest

Defence Science and Technology Organisation (DSTO), Edinburgh, S.A. 5111, Australia

DOI: 10.1109/JPHOT.2011.2106200

Manuscript received November 23, 2010; revised January 5, 2011; accepted January 7, 2011. Date of publication January 13, 2011; date of current version January 28, 2011. Corresponding author: M. Attygalle (e-mail: manik.attygalle@dsto.defence.gov.au).

Abstract: The design and experimental performance of a 40-GHz microwave photonic link scheme developed for broadband analog signal transmission that exhibits an increased input dynamic range compared with conventional microwave photonic links is presented. The scheme achieves an extension in the input power operating range by switching between two photonic links designed to operate at different input power levels, where the optical fiber provides the required delay for the switching operation. Although the extension in the dynamic range is noninstantaneous, the scheme has application in high-sensitivity receiver systems in a pulsed signal environment due to its feedforward gain control mechanism. This paper presents, through a realistic simulation study, the device parameter values required for optimized performance of a wideband (2–40 GHz) link with the noise figure, sensitivity, and dynamic range performance of each link and the composite link. A total "synthetic" dynamic range $>$ 100 dB with a minimum detectable signal of -110 dBm at a 100-kHz noise bandwidth can be achieved for the 2–40-GHz frequency range operation. The simulation results compare well with experimental results obtained with a practical implementation of the dual link architecture. The design and operational details of the switching circuitry required are also presented.

Index Terms: Optical fiber communication, radio frequency (RF) photonics, noise, electronic warfare (EW), electrooptic modulation.

1. Introduction

Micro/Milli-meter wave photonic links (MPL) offer a number of significant advantages over coaxial cable based microwave links in a variety of applications [1]. The advantages include low loss (0.2 dB/km) and weight, high bandwidth, and immunity to electromagnetic interference. Electronic warfare (EW) systems are one such example where MPLs can be used to connect spatially separated antenna/sensor elements to the sophisticated signal processing units. With the frequencies of modern radar systems ranging from sub-gigahertz up to millimeter-wave frequencies, the use of optical links with broad bandwidth will be desirable. However, the major barriers for the ubiquitous use of these links in these applications has been the relatively higher noise figure (NF) and limited dynamic range compared with coaxial cable links. These limitations are primarily due to the inefficient electric-to-optic and then optic-to-electric conversion, the added noise by the active photonic components and signal distortion due to nonlinear optical modulation.

A standard MPL consists of either a directly or externally modulated laser source, optional optical amplifier, optical fiber, and a photodiode. For high-frequency applications, external modulation using either a Mach–Zehnder modulator (MZM) or electroabsorption modulator is preferable, while

direct modulation can avoid the nonlinearity and optical power handling issues of external modulators. A variety of techniques have been presented so far to increase the dynamic range of MPLs. They include electrical and optical techniques for linearization with varying complexity [2]–[6], techniques that have focused on increasing the gain of the link by using high power lasers [7], optical amplification [8], [9] or increasing the optical power handling and linearity of the photo-detector (PD) [10]. Other methods include optical carrier suppression [11], [12] and low biasing of modulators [13] that improve the signal to average power levels incident on the PDs [14]. The latter methods however are more effective in the presence of optical amplification and sub-octave frequency ranges [15]. Furthermore, parallel modulator [16], [17], balanced detector [18], and coherent techniques [19], [20] have also been presented. All these methods have considerably improved the performance of analog optical links; however, the links may not still cover the full dynamic range required in some applications and can be limited in bandwidth and sensitivity. Also, most of these techniques require complex setups, highly sensitive operating points, or costly components. An excellent summary of performance limits of the conventional MPLs can be found in [7].

We recently developed a novel dual optical link architecture that can extend the input dynamic range of a wideband MPL using standard commercial off-the-shelf radio frequency (RF)-photonics components [21] where an initial design was briefly reviewed in [22]. The technique utilizes a parallel link topology with a high-sensitivity and low-sensitivity MPL. Switching logic is used to select which of the link outputs is most appropriate for the receiver, based on the detected power in the RF signal. This dual link architecture acts as a feedforward gain control mechanism with the optical fiber length providing the required delay for operation. Although the extension of the dynamic range is noninstantaneous, this system works well in a pulsed signal environment by switching to the low-sensitivity link (LSL) in the presence of high power pulses, avoiding signal compression in both the MPL and the receiver unit. The low loss delay provided by the optical links is an added functionality that overcomes any latency in the switching operation. This provides a "synthetic" extension of the dynamic range and provides an effective method to extend the input dynamic range of not only the photonic link but the receiver system as well.

This paper presents the detailed design and performance of the extended dynamic range (EDR)-MPL using a realistic simulation study and shows experimental results of an optimized implementation of wideband (2–40 GHz) EDR-MPL system developed for field trial. This paper is organized as follows. Section 2 describes the dual optical link architecture, while Section 3 gives the details of the simulation model. Section 4 presents the simulation results, together with the requirements for optimum implementation of the composite link. Section 5 gives consideration in the design of the detector circuit path with details of the switching operation. This is followed by experimental results of a practical implementation of the link in Section 6, together with further discussions. Finally, conclusions are given in Section 7.

2. Micro/Millimeter-Wave Photonic Dual Link Architecture

Fig. 1 shows the architecture of the EDR-MPL system consisting of two photonic links: one a high-sensitivity link (HSL) and the other an LSL. These links provide two different signal paths that are linked to a single output. The output from these links is selectively switched into either an analog or digital receiver for signal processing purposes. The input is initially amplified by a low noise amplifier (LNA) in order to lower the NF of the overall link. In the HSL, the majority of the RF signal power obtained through an RF directional coupler is modulated onto an optical carrier using an external MZM optical modulator. This signal can be further amplified by another LNA before modulation, and this link is designed to accommodate very low power RF signals, thereby defining the sensitivity of the EDR-MPL. For larger input power levels, however, the HSL undergoes saturation and distortion due to the nonlinear transfer function of the MZM and RF pre-amplifiers. In addition, at high input RF powers, the output power through an optimized optoelectronic link can exceed the maximum input power range in modern high-sensitivity EW digital receivers.

In the LSL, an attenuated RF signal from the directional coupler (−20 dB nominal) is used to modulate the MZM. This signal can be further attenuated by an RF attenuator. This link

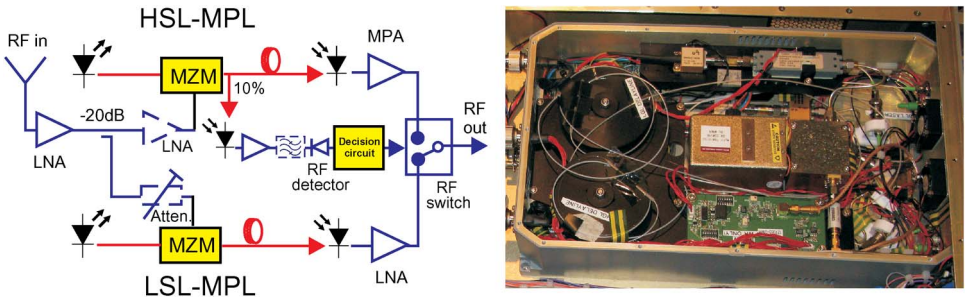

Fig. 1. Schematic for the EDR-MPL with dual link architecture showing the high sensitivity path (top), low sensitivity path (bottom), and detector path (middle). Also, shows a picture of the implementation of the transceiver.

accommodates larger input power levels without distortion, achieving this at the expense of sensitivity. The LSL therefore defines the upper limit of RF power that can be handled by the EDR-MPL. A switching logic circuit is used to redirect the appropriate signal channel into the receiver unit. Typically, a small proportion (5%–10%) of the optical power from the HSL will be tapped off into an RF-detector path to determine the signal power that activates the switching circuitry, while a short additional fiber spool (if the transmission fiber is not sufficient) can provide sufficient delay for the switching latency without significant loss in the signal. A switching time of < 250 ns can be achieved with standard commercial components, requiring a fiber length of 50 m, and can be further reduced, as discussed in Section 5. The output of the HSL can then be amplified by a microwave power amplifier (MPA) to extend the operational power window of this link without output RF signal saturation. On the other hand, the LSL can be amplified by a LNA with higher gain to compensate for the earlier losses before optical modulation that will also reduce further addition of noise.

3. Description of Simulations

The aim of the simulation was to investigate the architecture, components and device parameter values required to provide the optimum dynamic range and noise performance for the EDR-MPL. Different scenarios were evaluated for the HSL and LSL that had different amplification and attenuation. The HSL can have up to 60 dB pre-amplification in its path before the modulator utilizing the two RF amplifiers (before and after the RF coupler). The LSL can have different attenuations in its path after the -20 dB coupler. These variable modules are shown in dashed lines in Fig. 1. In addition, at the output of the PDs, the HSL and LSL can have either a MPA or a LNA for post-detection RF amplification.

The numerical simulation was carried out using commercial photonic software, i.e., VPITransmissionmaker, with its tested optical modules, and took into account a range of typical photonic and RF component parameters as detailed in Table 1. The RF amplifiers were simulated using additional white noise sources and signal processing modules that gave accurate operational characteristics. The relative intensity noise (RIN) of lasers is specified at a measurement power of 50 mW and will inversely vary with the laser output power which mimic the behavior of a typical laser.

A 1-MHz frequency resolution was selected for the simulation as a compromise between resolution and simulation time. This also takes into account the performance requirements of the digital receiver to be used for processing of the received signals, which requires signals to be approximately 10 dB above the noise floor in a 100-kHz bandwidth. Since the final instantaneous operation of the receiver was limited to a single octave, second-order distortions due to modulator bias drifts and component nonlinearity was ignored. The RF amplifier bandwidth was limited to 2–40 GHz that will dictate the total thermal noise power; however, a gain roll-off for individual components over the bandwidth was not included as the aim was to identify nominal gain for the components. The MZM were biased at quadrature, and a 3-dB additional optical loss was also assumed for connector/splice and fiber losses. To obtain the dynamic range, a two-tone simulation was carried out for a signal with 100-MHz frequency separation applicable to frequencies from 2–40 GHz.

TABLE 1

Variable parameters and the value ranges used in simulation

Variable	Range	Units
Laser relative intensity noise (RIN)	-120 to -170	dB/Hz @ 50 mW
Laser Power	25 to 100	mW
Linewidth	2 to 10	MHz
MZM $V\pi$ (RF)	3 to 7	V
MZM insertion loss	3 to 6	dB
MZM extinction	15 to 30	dB
PD responsivity	0.5 to 0.93	A/W
PD dark current	10	nA
PD thermal noise	10	pA $\sqrt{Hz}$
RF amplifier gain	15 to 35	dB
RF amplifier NF	2.5 to 7	dB
RF amp output saturation power	10 to 25	dBm

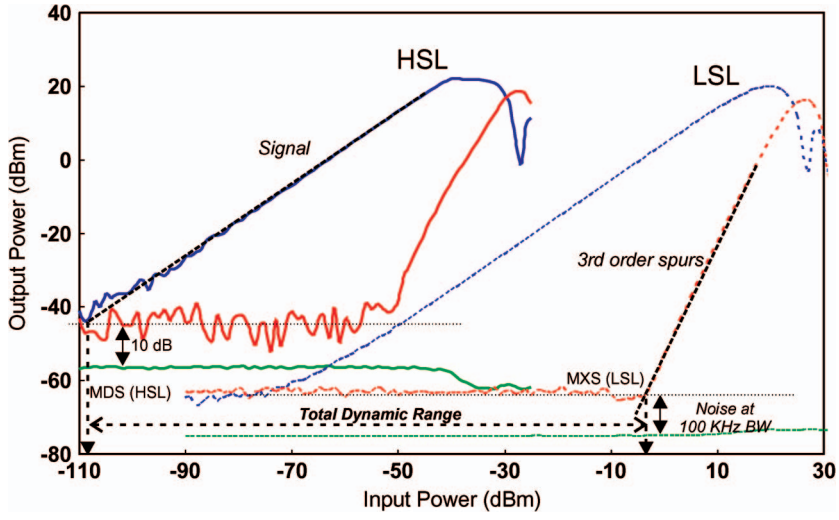

Fig. 2. Output power versus Input power for typical HSL (solid line) and LSL (dashed line). The figure also depicts the defined MDS and MXS parameters in the HSL and LSL, respectively.

4. Simulation Results

Fig. 2 shows an example input-output response for the HSL (solid line) and the LSL (dashed line) that diagrammatically explains the concept. It shows the output signal power, noise power (in 100 kHz bandwidth), and power of the third-order spurious products. The HSL is constrained at the lower input power end by the signal-to-noise ratio (SNR) requirement and the high input power end the by the onset of output signal compression and saturation of the RF post-amplifier at high input RF powers. The switching logic will switch to the output from the LSL at some pre-determined point before this occurs. Similarly, the LSL will be constrained by the onset of spurious signals due to MZM nonlinearity and saturation of the RF pre-amplifier.

In this paper, the minimum detectable signal (MDS) is defined as the input power value for which the output power is 10 dB above the noise floor (in 100-kHz bandwidth). Consistent with the MDS, the maximum input signal (MXS) is defined as input power value when the spurious signal power is 10 dB above the noise power. In order to extend the input dynamic range of the EDR-MPL, the MDS of the HSL should be reduced by increasing the sensitivity of the HSL. Likewise, the MXS of the LSL should be increased by delaying the onset of spurs, while keeping an appropriate overlap between the two responses so that switching between the HSL and LSL can be performed seamlessly and without signal loss or degradation. In other words, the MXS of the HSL needs to be larger than the MDS of the LSL (typically in the range of 10 dB). The total “synthetic” dynamic range of the

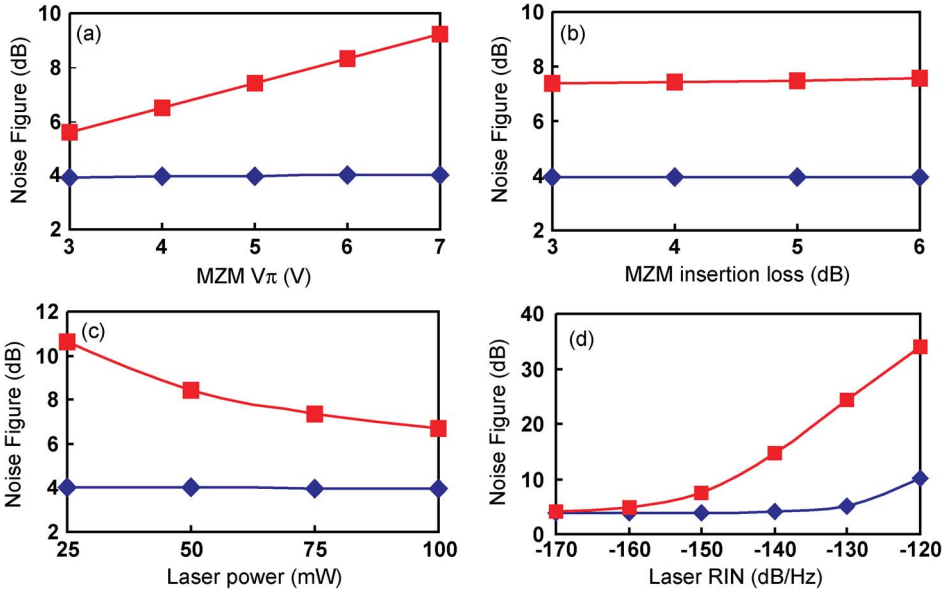

Fig. 3. Noise figure for the HSL against (a) MZM half-wave switching voltage (b) MZM insertion loss (c) laser power and (d) laser RIN. The diamonds represent a HSL with two cascaded pre-amplifiers with 30-dB gain each and squares are for a HSL with one 35-dB pre-amplifier.

EDR-MPL is the input power range between the MDS of the HSL and the MXS of the LSL, as depicted in Fig. 2. In the next subsections, the HSL and LSL are analyzed separately to evaluate the effects of different component parameters on the composite link performance.

4.1. HSL

Fig. 3 shows the NF of the HSL when (a) the MZM $V\pi$, (b) MZM insertion loss, (c) laser power, and (d) laser RIN is varied, respectively, with all other parameters kept constant (laser linewidth $=$ 5 MHz, laser power $=$ 75 mW, RIN $=-150$ dB/Hz @ 50 mW, MZM $V\pi = 5$ V, MZM insertion loss $=$ 4 dB, MZM extinction $=$ 25 dB, PD responsivity $=$ 0.7 A/W, and NF of RF amplifiers $=$ 4 dB). The diamond symbols in the figure indicate the HSL with 60-dB RF pre-amplification, while the square symbols depict when the gain is 35 dB. Note that the $V\pi$ is the half-wave switching voltage of the optical modulator, and the NF of the overall link is calculated rather than the NF of the optical section alone to give better comparisons with coaxial cable based RF links.

From Fig. 3 it can be seen that the NF of the HSL with the higher RF pre-gain (resulting from a cascaded RF amplifier configuration) is governed by the noise performance of the amplifiers (NF $=$ 4 dB), as expected. There is a NF penalty only when the RIN of the laser is above -140 dB/Hz. On the other hand, the NF varies with the optical component values when there is lower RF gain before the modulator. In this case, as in a typical MPL, a smaller $V\pi$ and higher laser power produces the best noise performance as the NF of the optical part of the link has a significant effect on the overall NF [7].

Fig. 4 shows the MDS for the HSL when (a) the MZM $V\pi$ and (b) MZM insertion loss is varied with other parameters kept constant, as before. It is observed that the MDS can be maintained at -110 dBm with a higher RF pre-gain in the HSL while the MDS is reduced to around -107 dBm with lower RF gain. It also indicates that when higher pre-amplification is used, the stringent requirements of the optical components such as low MZM $V\pi$ and low laser RIN can be relaxed, which can lead to lower implementation cost.

In summary, we note as expected, that larger pre-amplifier gain will lead to lower NF of the HSL and, hence, the best sensitivity. However, having very high gain at the antenna units can be disadvantageous due to power consumption, heat dissipation, and the generation of spurious signals due to the second amplifier saturation. It is therefore appropriate to use the lowest gain that

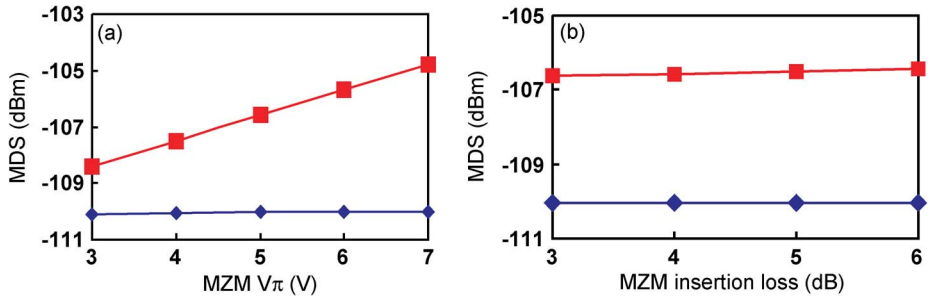

Fig. 4. MDS for the HSL against (a) MZM half-wave switching voltage and (b) MZM insertion loss. The diamonds represent the HSL with two cascaded pre-amplifiers with 30-dB gain each, and the squares represent the HSL with one 35-dB pre-amplifier.

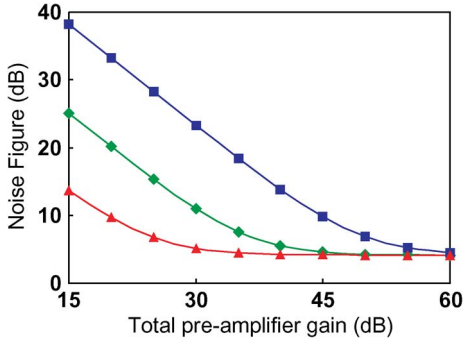

Fig. 5. NF against pre-amplifier gain for three different scenarios for the optical components with best- to worse-case component specification from triangles and diamonds to squares.

gives the required NF performance. However, this will depend on the noise performance of the optical part of the link when different optical components are used.

Fig. 5 shows the overall NF for three cases of optical component variables. The triangles depict a best-case scenario where laser power = 100 mW, RIN = −160 dB/Hz @ 50 mW, MZM $V\pi = 4$ V, MZM insertion loss = 3 dB, MZM extinction = 30 dB, and PD responsivity = 0.9 A/W. In this case, the overall NF will start to asymptote toward the pre-amplifier NF at around a 35-dB gain. The diamonds depict a second case for the optical parameter values as given at the beginning of this section (laser power = 75 mW, RIN = −150 dB/Hz @ 50 mW, MZM $V\pi = 5$ V, MZM insertion loss = 4 dB, MZM extinction = 25 dB, and PD responsivity = 0.7 A/W). In this case, reasonable pre-amplification is around 40 dB. The squares depict a worst-case scenario where the laser power = 50 mW, RIN = −140 dB/Hz @ 50 mW, MZM $V\pi = 6$ V, MZM insertion loss = 5 dB, MZM extinction = 15 dB, and PD responsivity = 0.5 A/W. In this case, much higher pre-amplifier gain is required (∼55 dB) to decrease the NF close to the 4-dB mark. This is simply due to the increase in the NF and the RF loss in optical part of the link when optical components are not the optimum. Therefore, higher pre-amplification will be required to reduce the overall NF of the system. These results were confirmed by results from an analytical model where the NF and the loss of the optical link alone was obtained using an analytical model [1] and the overall NF is calculated by substituting this into the Friis equation with the gain and NF of the pre- and post-amplification stages. The very similar results obtained show the validity of the numerical simulation.

4.2. LSL

For the LSL, a 25-dB LNA was assumed before the −20-dB coupler. This gain value was a compromise between lowering the NF and saturation of the amplifier due to high powered signals. With commercial broadband amplifiers, the output power should be typically limited to

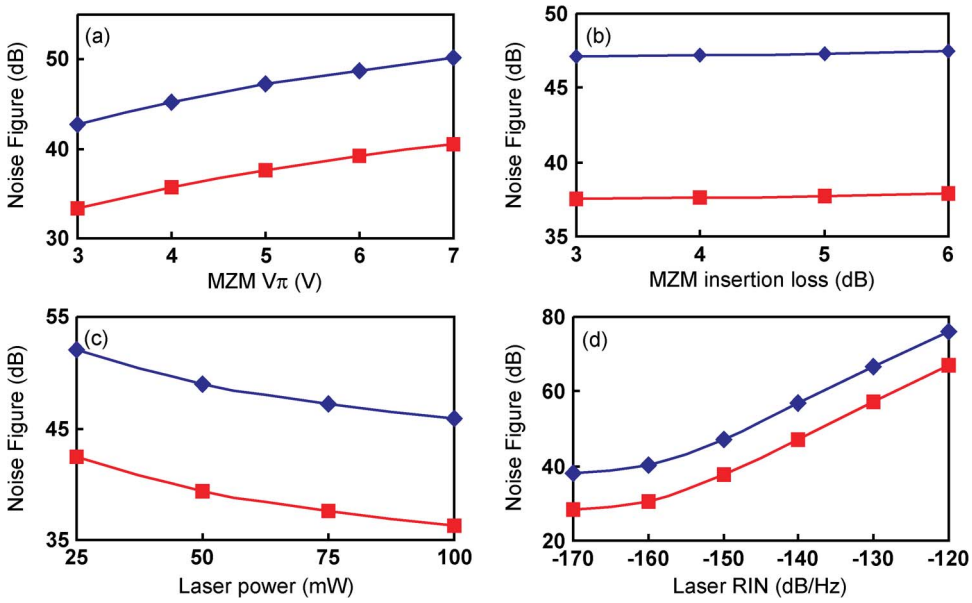

Fig. 6. Noise figure for the LSL against (a) MZM half-wave switching voltage, (b) MZM insertion loss, (c) laser power, and (d) laser RIN. The squares represent an LSL with the −20-dB coupler and diamonds with an additional 10-dB attenuator after the coupler.

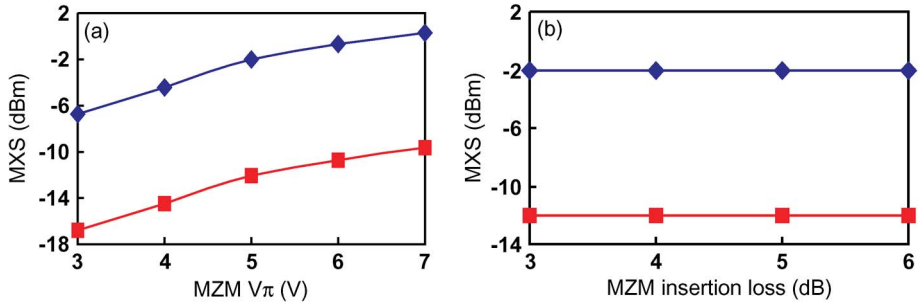

Fig. 7. MXS for the LSL against (a) MZM half-wave switching voltage and (b) MZM insertion loss. The diamonds represent an LSL with a 10-dB attenuator, and squares represent an LSL with no attenuation.

approximately +10 dBm before degradation due to spurious signals. Hence, the LSL will function up to −15 dBm input power signals with negligible spurious signals due to output compression. Fig. 6 shows the NF for the LSL when (a) MZM $V\pi$, (b) MZM insertion loss, (c) laser power, and (d) laser RIN is varied with other parameters kept constant, as in Section 4.1. The diamond symbols represent an LSL with a 10-dB attenuator after the coupler, and the squares represent an LSL with no attenuator. The NF of the LSL is significantly larger than the HSL, and the effects of the laser power and RIN are more pronounced. However, it should be noted that the function of the LSL is to increase the MXS while maintaining reasonable noise performance. Also, the larger the attenuation, the larger the NF as well as the shift in the LSL output curves to the right, as shown in Fig. 2. It will ultimately lead to complete separation of outputs from the HSL and LSL, and there will be no input power overlap for the switching operation. This will lead to a loss of signal within some input power range. Hence, too large a power difference between the HSL and LSL needs to be avoided.

Fig. 7 shows the MXS for the LSL when (a) the MZM $V\pi$ and (b) MZM insertion loss is varied with other parameters kept constant as before. The MXS is approximately −20 dBm with no attenuator and −10 dBm when a 10-dB attenuator is used after the coupler. As expected, the MXS is larger by 10 dB when a 10-dB attenuator is used. Furthermore, we also note that larger $V\pi$ will give larger

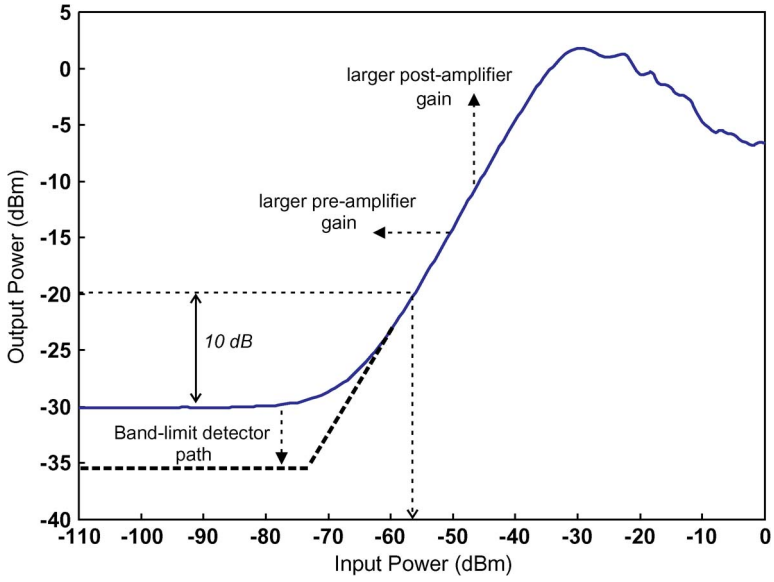

Fig. 8. Power into RF detector showing the minimum power level at which reliable switching can be achieved.

MXS, while the insertion loss of the MZM does not have a significant effect on the MXS of the link. As a result, a MZM with larger $V\pi$ will be preferable for the LSL to increase the power level without distortion of the signal. From these simulation results, the optimum pre-amplification for the HSL can be inferred to be 45 dB. This will provide a low NF with reasonable optical components. Also, as mentioned before, with the selection of pre-amplification for the HSL and the attenuation for the LSL, there must be operational input power level overlap between the two links. The MDS for the LSL with the 10-dB attenuator was measured to be -72 dBm, while the MXS for the HSL with 45 dB pre-amplification was -51 dBm, which gives the required $>$ 10 dB input power range overlap between the two links needed to achieve switching. Note that with 45 dB total pre-gain for the HSL, the maximum power difference between the HSL and LSL is limited to 60 dB in order to satisfy the 10-dB input power range overlap condition. Therefore, in this scenario, the maximum attenuator that can be inserted after the coupler will be 20 dB.

5. Detector Circuit

The RF detector circuit path consists of a photodiode, RF amplifier, optional narrow band filter, RF detector, optional log video amplifier, high-speed comparator circuit and switch driver circuit which generate a TTL control signal for the SP2T diode switch. If the dual link is designed to have large power difference between the HSL and LSL in order to obtain larger ($>$ 50 dB) isolation for the LSL from the HSL, a SPST switch can be cascaded at each output of the two-way switch, which are then controlled by the same switching control circuit.

Due to the broad bandwidth of the detection path, there is a lower power limit where reliable switching can be achieved due to the high noise power into the RF detector. A reliable switching point is assumed to be at 10 dB SNR. Furthermore, to generate signals with sufficient voltage from the detector used in the experiment, approximately -20 dBm RF power is required into the RF detector at the switching trigger power point. These conditions put a lower input power limit for switching between links. Fig. 8 shows the total power into the RF detector versus input power for an HSL with 45 dB pre-amplification assuming 10% optical power tapped for the detection circuit. The figure shows that the aforementioned conditions are satisfied by the output signal and is achieved with a 25-dB RF gain in the detector path after the photodiode. With this setting, the minimum input power at which the detector circuit can achieve reliable switching is approximately -57 dBm input

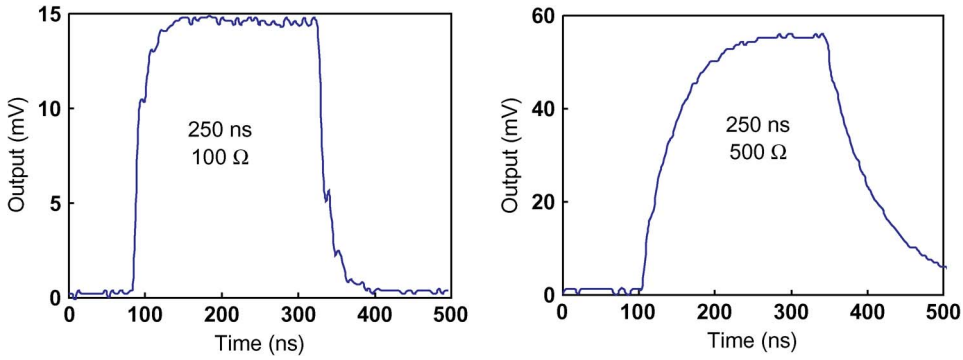

Fig. 9. Detected pulses with 250 pulse width showing pulse amplitude and rise-time variation with output impedance.

power. The sensitivity and the operating region of the detector path can be changed by the pre-amplifier gain or the post RF amplification. If better sensitivity is required, the detector circuit path can be band limited to frequency ranges where high power pulses are expected and was carried out in the implementation.

A suitable fiber length should also be selected for both HSL and LSL to accommodate sufficient delay for the switching latency. This was calculated to be 50 m of single mode fiber that will provide $>$ 240 ns of delay. This delay was computed by considering the following 10/20% to 80/90% rise times of each stage. RF detector (50 ns), comparator (10 ns), switch driver (5 ns), RF switch (150 ns), and additional 10% delay for variations. This is a conservative assumption for low power pulses that will just trigger the switching. With high power pulses, the decision circuit may work faster due to a faster slew rate. Finally, it is noted that a more sophisticated signal processing technique can be employed for the decision circuitry where the switch decision is made using both RF power levels from the HSL and LSL rather than power level only from the HSL; however, it is not discussed here.

6. Experimental Measurements

A ruggedized 40-GHz EDR-MPL was implemented with state-of-the-art commercially available components that could be field trialed. The input signals from two cavity backed circular polarized antenna elements with operation in microwave and mm-wave frequency regions were passed through RF limiters and separate microwave and millimeter-wave LNAs with $\sim$20-dB gain. The separate amplification bands can provide a mechanism to equalize the higher frequency roll-off in subsequent components by having larger amplification at higher frequency bands. After a combination of the microwave and millimeter-wave signal paths, the resultant broadband signal is passed through an RF coupler ($-$13 dB) and is split into the HSL and LSL paths. The HSL signal is further amplified by a broadband RF amplifier (28-dB gain). Therefore, the gain difference between the HSL and LSL is $>$ 40 dB. The two signals with the different power level are modulated onto two optical carriers using 40-GHz modulators (EOSPACE-Z cut) and transmitted via the optical fibers and detected by two high speed PDs with responsivity of $\sim$0.65 A/W and high optical power handling (16 dBm). One percent optical taps are used for bias control of the modulators, and another 10% optical tap from the HSL path is used for the detector path that activates the switch. The DFB laser had an output power of 20 dBm at a wavelength of $\sim$1550 nm. The detector path consisted of a 2–18-GHz post amplifier, optional narrowband Yttrium Iron Garnet (YIG) microwave filter ($<$ 1 GHz), 40-GHz RF detector, and the detector circuitry. The frequency range in the detector path was limited to 2–18 GHz as high power signals were expected only within this frequency range. The YIG provided further narrowing of the frequency range to the detection circuitry that further increases the sensitivity of the switching operation. The HSL and LSL optical path also consists of 50-m optical fiber reels to give necessary time delay for the switching latency.

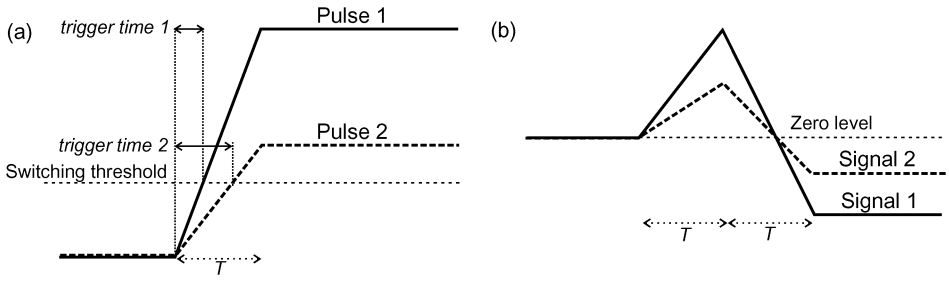

Fig. 10. Diagram depicting (a) the trigger time variance and (b) reduced variance through zero-crossing detection.

TABLE 2

Experimental results

Link	Gain (dB) 10 GHz	Gain (dB) 35 GHz	NF(dB) 10 GHz	NF (dB) 26.5 GHz	SFDR (dB @ 100 kHz BW) 10 GHz
HSL	49	43	4.05	4.1	69
LSL	4	-0.5	26.5	27	85

The RF detector output amplitude and rise-time depends on the output impedance, as shown in Fig. 9, due to the component RC time constant. As expected, with larger output impedance, we obtain larger amplitude but slower rise-time. Approximately 450 Ω was selected as a compromise between sensitivity of detection and rise-time. The detector circuit consists of a high-speed comparator stage with adjustable threshold and hysteresis at the threshold, as well as a switch driver. The 40-GHz RF switch used has 5 dB insertion loss and an isolation of -60 dB. Typical measured switching time for the switch was 100 ns, and there is about an additional 15-ns delay in the comparator and the logic circuitry. This leads to a lower bound of the switch time to $\sim$150 ns which includes the trigger time, which is the time it takes to initiate the switch operation from pulsed input as diagrammatically shown in Fig. 10(a). A small variation of this trigger time was observed with a different level of pulse amplitudes that triggers the switching, as depicted in Fig. 10. When the signal pulse is very large, the trigger time could be as low as a few tens of nanoseconds. It is observed that this trigger time can increase to close to 100 ns with low pulse amplitudes where the detected signal level is very close to the switching threshold. The hysteresis avoids toggling of the switch due to noise. The 50-m fiber length selected was sufficient to allow for the largest delay in switching operation. It is noted that this switch time variance can be reduced considerably with the use of faster rise time detectors based on tunnel diodes with rise times of 5 ns, which are commercially available. This will also reduce the switching latency to $<$ 150 ns. Further, the amplitude dependent switching jitter can be reduced by a zero-crossing detection scheme where the pulse is split into two unequal paths, delaying one part by the total rise time and combining. The zero crossing point will have much lower time variance due to change in amplitude, as shown in Fig. 10(b). The experimental switching power range was -62 dBm to -70 dBm, which was adjusted to avoid saturation of the ADC units in the receiver. Note the range is lower compared with the discussion in Section 5 due to the smaller frequency range in the detection path.

The measured gain and NF of the HSL and LSL is shown in Table 2 at two different frequencies. Lower gain at millimeter-wave frequency is due to component response roll-off, and as mentioned earlier, this can be overcome by having larger gain millimeter-wave amplifier in the front end. The SFDR at 100 kHz was measured using the third-order intercept point (IP3) obtained through two tone measurements with the two frequencies at 10 and 10.1 GHz. The total dynamic range with the switching operation was measured to be 117 dB at 100 kHz noise bandwidth, which extends the dynamic range of a conventional photonic link by $>$ 30 dB at this bandwidth. The measured phase

noise of the links varied from −131 dBc/Hz to −118 dBc/Hz @ 500 kHz offset across the 2–40 GHz frequency band.

This scheme may offer an effective method to increase the dynamic range of modern EW digital receiver systems. This dual photonic link architecture acts as a feedforward automatic gain control mechanism that can align two input power regions into a single input power range required by the receivers, with the fiber length providing the required delay for operation. This is the advantage of photonics as it is difficult to achieve this functionality with electronic techniques either using fast attenuators or electrical delays. Although the increase in the input dynamic range is non-instantaneous, the system should be particularly effective in low-to-medium density high-power pulsed environments. As with most feedforward gain control techniques, a limitation of this system is blinding of low power signals when the link operates in the low-sensitivity mode. However, the link will operate in the low-sensitivity mode only during the presence of a high power pulse. In addition, utilization of filter banks can further increase the versatility of the system.

7. Conclusion

This paper presented the design and experimental performance of an extended dynamic range MPL that is suitable for analog signal-remoting applications. The MPL consists of a parallel link topology consisting of an HSL defining the minimum detectable signal power and an LSL that defines the maximum input power. A detailed simulation study optimized the extended dynamic range of a 40-GHz link by changing the variables within practical limits of commercially available components. The optimum EDR-MPL was observed to be an HSL with two cascaded pre-amplifiers having a combined RF gain of 45 dB coupled with a MZM with lower half-wave switching voltage and an LSL with one low gain RF pre-amplifier (25 dB), a 10-dB attenuator after the RF coupler (−20 dB) that splits the signal into the two paths, and an MZM with a higher switching voltage. A total "synthetic" dynamic range of more than 100 dB at 100 kHz noise bandwidth can be achieved with the MDS at −110 dBm and the MXS above −10 dBm using this EDR-MPL configuration. A practical dual link architecture was implemented with commercial off-the shelf components with 40-GHz bandwidth operation. Measurement of the system showed expected characteristics with the switching operation increasing the input power range into an EW digital receiver system. The design and results presented practical considerations in the switching signal path. These links can play a useful role in both analog and digital EW systems, especially in high-power pulsed environments where large dynamic range operation is required.

Acknowledgment

The authors would like to thank D. McManus, T. Lindsay, R. Lindop, M. Manka, A. Sarti, P. Davies, D. Hunter and M. Parker for helpful discussions.

References

[1] C. H. Cox, III, *Analog Optical Links*. Cambridge, U.K.: Cambridge Univ. Press, 2004. [Online]. Available: http://dx.doi.org/10.1017/CBO9780511536632

[2] Y. Chiu, B. Jalali, S. Garner, and W. Steier, "Broad-band electronic linearizer for externally modulated analog fiber-optic links," *IEEE Photon. Technol. Lett.*, vol. 11, no. 1, pp. 48–50, Jan. 1999.

[3] T. Ismail, C.-P. Liu, J. Mitchell, and A. Seeds, "High-dynamic-range wireless-over-fiber link using feedforward linearization," *J. Lightw. Technol.*, vol. 25, no. 11, pp. 3274–3282, Nov. 2007.

[4] V. Urick, M. Rogge, P. Knapp, L. Swingen, and F. Bucholtz, "Wide-band predistortion linearization for externally modulated long-haul analog fiber-optic links," *IEEE Trans. Microw. Theory Tech.*, vol. 54, no. 4, pp. 1458–1463, Jun. 2006.

[5] S. O'Connor, T. Clark, and D. Novak, "Wideband adaptive feedforward photonic link," *J. Lightw. Technol.*, vol. 26, no. 15, pp. 2810–2816, Aug. 2008.

[6] B. Dingel, "Ultra-linear, broadband optical modulator for high performance analog fiber link system," in *Proc. IEEE MWP*, Oct. 2004, pp. 241–244.

[7] C. Cox, III, E. Ackerman, G. Betts, and J. Prince, "Limits on the performance of rf-over-fiber links and their impact on device design," *IEEE Trans. Microw. Theory Tech.*, vol. 54, no. 2, pp. 906–920, Feb. 2006.

[8] A. Karim and J. Devenport, "Noise figure reduction in externally modulated analog fiber-optic links," *IEEE Photon. Technol. Lett.*, vol. 19, no. 5, pp. 312–314, Mar. 2007.

[9] V. Urick, M. Rogge, F. Bucholtz, and K. Williams, "The performance of analog photonic links employing highly compressed erbium-doped fiber amplifiers," *IEEE Trans. Microw. Theory Tech.*, vol. 54, no. 7, pp. 3141–3145, Jul. 2006.
[10] K. Williams, D. Tulchinsky, and J. Campbell, "High-power photodiodes," in *Proc. IEEE MWP*, Oct. 2007, pp. 9–13.
[11] M. LaGasse, W. Charczenko, M. Hamilton, and S. Thaniyavarn, "Optical carrier filtering for high dynamic range fibre optic links," *Electron. Lett.*, vol. 30, no. 25, pp. 2157–2158, Dec. 1994.
[12] R. Esman and K. Williams, "Wideband efficiency improvement of fiber optic systems by carrier subtraction," *IEEE Photon. Technol. Lett.*, vol. 7, no. 2, pp. 218–220, Feb. 1995.
[13] M. Farwell, W. Chang, and D. Huber, "Increased linear dynamic range by low biasing the Mach–Zehnder modulator," *IEEE Photon. Technol. Lett.*, vol. 5, no. 7, pp. 779–782, Jul. 1993.
[14] C. Lim, M. Attygalle, A. Nirmalathas, D. Novak, and R. Waterhouse, "Analysis of optical carrier-to-sideband ratio for improving transmission performance in fiber-radio links," *IEEE Trans. Microw. Theory Tech.*, vol. 54, no. 5, pp. 2181–2187, May 2006.
[15] M. M. Sisto, S. LaRochelle, and L. A. Rusch, "Gain optimization by modulator-bias control in radio-over-fiber links," *J. Lightw. Technol.*, vol. 24, no. 12, pp. 4974–4982, Dec. 2006.
[16] S. Korotky and R. de Ridder, "Dual parallel modulation schemes for low-distortion analog optical transmission," *IEEE J. Sel. Areas Commun.*, vol. 8, no. 7, pp. 1377–1381, Sep. 1990.
[17] T. Darcie and P. Driessen, "Class-AB techniques for high-dynamic-range microwave-photonic links," *IEEE Photon. Technol. Lett.*, vol. 18, no. 8, pp. 929–931, Apr. 2006.
[18] M. Saiful Islam, T. Chau, S. Mathai, T. Itoh, M. Wu, D. Sivco, and A. Cho, "Distributed balanced photodetectors for broad-band noise suppression," *IEEE Trans. Microw. Theory Tech.*, vol. 47, no. 7, pp. 1282–1288, Jul. 1999.
[19] D. Sabido, IX, M. Tabara, T. Fong, C.-L. Lu, and L. Kazovsky, "Improving the dynamic range of a coherent am analog optical link using a cascaded linearized modulator," *IEEE Photon. Technol. Lett.*, vol. 7, no. 7, pp. 813–815, Jul. 1995.
[20] A. Ramaswamy, L. Johansson, J. Klamkin, H.-F. Chou, C. Sheldon, M. Rodwell, L. Coldren, and J. Bowers, "Integrated coherent receivers for high-linearity microwave photonic links," *J. Lightw. Technol.*, vol. 26, no. 1, pp. 209–216, Jan. 2008.
[21] T. Lindsay, R. Lindop, K. Gupta, R. Nicks, D. Palumbo, T. Priest, and A. Vanderklugt, "Photonic link with improved dynamic range," Patent WO/2006/128 250, Dec. 7, 2006.
[22] M. Attygalle, T. Priest, K. Gupta, and D. Hunter, "Performance of an extended input power range microwave photonic link with dual link architecture," in *Proc. Microw. Photon.*, Sep. 2008, pp. 158–161.